LAWRENCE
LIVERMORE
NATIONAL
LABORATORY

LLNL-JRNL-819741

Burning plasma achieved in inertial fusion

A. B. Zylstra, O. A. Hurricane, D. A. Callahan, A. L. Kritcher, J. Ralph, H. F. Robey, J. S. Ross, C. Young, K. Baker, D. T. Casey, T. Doeppner, L. Divol, M. Hohenberger, S. Le Pape, A. Pak, P. Patel, R. Tommasini

February 22, 2021

Nature

Disclaimer

LLNL-JRNL-819741

Article

Burning plasma achieved in inertial fusion

A. B. Zylstra[1,*], O. A. Hurricane[1,*], D. A. Callahan[1], A. L. Kritcher[1], J. E. Ralph[1], H. F. Robey[2], J. S. Ross[1], C. V. Young[1], K. L. Baker[1], D. T. Casey[1], T. Döppner[1], L. Divol[1], M. Hohenberger[1], S. Le Pape[3], A. Pak[1], P. K. Patel[1], R. Tommasini[1], S. J. Ali[1], P. A. Amendt[1], L. J. Atherton[1], B. Bachmann[1], D. Bailey[1], L. R. Benedetti[1], L. Berzak Hopkins[1], R. Betti[4], S. D. Bhandarkar[1], R. M. Bionta[1], N. W. Birge[2], E. J. Bond[1], D. K. Bradley[1], T. Braun[1], T. M. Briggs[1], M. W. Bruhn[1], P. M. Celliers[1], B. Chang[1], T. Chapman[1], H. Chen[1], C. Choate[1], A. R. Christopherson[1], D. S. Clark[1], J. W. Crippen[5], E. L. Dewald[1], T. R. Dittrich[1], M. J. Edwards[1], W. A. Farmer[1], J. E. Field[1], D. Fittinghoff[1], J. Frenje[6], J. Gaffney[1], M. Gatu Johnson[6], S. H. Glenzer[7], G. P. Grim[1], S. Haan[1], K. D. Hahn[1], G. N. Hall[1], B. A. Hammel[1], J. Harte[1], E. Hartouni[1], J. E. Heebner[1], V. J. Hernandez[1], H. Herrmann[2], M. C. Herrmann[1], D. E. Hinkel[1], D. D. Ho[1], J. P. Holder[1], W. W. Hsing[1], H. Huang[5], K. D. Humbird[1], N. Izumi[1], L.C. Jarrott[1], J. Jeet[1], O. Jones[1], G. D. Kerbel[1], S. M. Kerr[1], S. F. Khan[1], J. Kilkenny[5], Y. Kim[2], H. Geppert Kleinrath[2], V. Geppert Kleinrath[2], C. Kong[5], J. M. Koning[1], J. J. Kroll[1], O. L. Landen[1], S. Langer[1], D. Larson[1], N. C. Lemos[1], J. D. Lindl[1], T. Ma[1], M. J. MacDonald[1], B. J. MacGowan[1], A. J. Mackinnon[1], S. A. MacLaren[1], A. G. MacPhee[1], M. M. Marinak[1], D. A. Mariscal[1], E. V. Marley[1], L. Masse[1], K. Meaney[2], N. B. Meezan[1], P. A. Michel[1], M. Millot[1], J. L. Milovich[1], J. D. Moody[1], A. S. Moore[1], J. W. Morton[8], T. Murphy[2], K. Newman[1], J.-M. G. Di Nicola[1], A. Nikroo[1], R. Nora[1], M. V. Patel[1], L. J. Pelz[1], J. L. Peterson[1], Y. Ping[1], B. B. Pollock[1], M. Ratledge[5], N. G. Rice[5], H. Rinderknecht[4], M. Rosen[1], M. S. Rubery[8], J. D. Salmonson[1], J. Sater[1], S. Schiaffino[1], D. J. Schlossberg[1], M. B. Schneider[1], C. R. Schroeder[1], H. A. Scott[1], S. M. Sepke[1], K. Sequoia[5], M. W. Sherlock[1], S. Shin[1], V. A. Smalyuk[1], B. K. Spears[1], P. T. Springer[1], M. Stadermann[1], S. Stoupin[1], D. J. Strozzi[1], L. J. Suter[1], C. A. Thomas[4], R. P. J. Town[1], E. R. Tubman[1], P. L. Volegov[2], C. R. Weber[1], K. Widmann[1], C. Wild[9], C. H. Wilde[2], B. M. Van Wonterghem[1], D. T. Woods[1], B. N. Woodworth[1], M. Yamaguchi[5], S. T. Yang[1], G. B. Zimmerman[1]

[1] Lawrence Livermore National Laboratory, P.O. Box 808, Livermore, California 94551-0808, USA
[2] Los Alamos National Laboratory, Mail Stop F663, Los Alamos, New Mexico 87545, USA
[3] Laboratoire pour l'utilisation des Lasers Intenses chez École Polytechnique, F-91128 Palaiseau cedex, France
[4] Laboratory for Laser Energetics, University of Rochester, Rochester, New York 14623, USA
[5] General Atomics, San Diego, California 92186, USA
[6] Massachusetts Institute of Technology, Cambridge, Massachusetts 02139, USA
[7] SLAC National Accelerator Laboratory, Menlo Park, California 94025, USA
[8] Atomic Weapons Establishment, Aldermaston, RG7 4PR, United Kingdom
[9] Diamond Materials Gmbh, 79108 Freiburg, Germany
[*] these authors contributed equally: A.B. Zylstra, O.A. Hurricane

Obtaining a burning plasma is a critical step toward self-sustaining fusion energy[1]. A burning plasma is one in which the fusion reactions themselves are the primary source of heating in the plasma, which is necessary to sustain and propagate the burn, enabling high energy gain. After decades of fusion research, a burning plasma state has been achieved in the laboratory. These experiments were conducted on the National Ignition Facility, a laser facility delivering up to 1.9MJ of energy in pulses with peak powers up to 500TW; we use the lasers to generate x rays in a radiation cavity to indirectly drive a fuel-containing capsule via the x-ray ablation pressure, the implosion process compresses and heats the fuel via mechanical work. We report upon these first burning-plasma experiments; this state was created using a strategy to increase the capsule spatial-scale[2,3] via two different implosion concepts[4–7]. These experiments show fusion self-heating in excess of the mechanical work injected into the implosions satisfying several burning plasma metrics[3,8], additionally a subset of recent experiments appear to have crossed the self-heating boundary, where fusion heating surpasses energy losses from radiation and conduction. The resulting alpha-dominated plasmas provide an invaluable platform to study burning plasma physics for the first time.

Fusion research fundamentally aims to create a system that produces more energy than was required to create it, a necessary condition for energy applications; in practice the fusion reaction must be self-sustaining with self-heating overtaking loss mechanisms, termed 'ignited' [9]. Such conditions are reached in astrophysical objects including the cores of stars, novae, and type 1a supernovae, and in thermonuclear weapons. Ignition in the laboratory requires heating the fuel to incredibly high temperatures, where it becomes a 'plasma' and fusion reactions readily occur, while also controlling energy losses. Several approaches have been developed to heat and confine plasma over the last several decades, with most pursuing deuterium-tritium (DT) fuel, which is the easiest to get to ignition. The dominant approaches to plasma confinement are 'inertial', an impulsive burn while the fuel is confined by its own inertia, and 'magnetic', in which specialized configurations of magnetic fields provide confinement to the charged particles in the plasma. In order for a DT fusion [$D + T \rightarrow \alpha$ (3.5 MeV) + n (14 MeV)] plasma to become thermally unstable and ignite, it must first obtain a 'burning' state. In this regime, self-heating from α-particle deposition exceeds the external heating input into the DT;[8] this ratio is denoted Q_α where the self-heating is taken relative to the heating power to the plasma, for inertial fusion this is the PdV compressional work on the fuel and not the total laser energy. $Q_\alpha > 1$ is a burning plasma.

A burning plasma state signifies a transformational change to the energy and power balance in the DT plasma, opening up the potential for rapidly increasing performance. In the impulsive case of inertial confinement fusion (ICF)[10], Q_α can be stated either as a power during burn, or as an energy integrated over the burn duration, while for the

near steady-state operation of magnetic fusion energy (MFE), Q_α is a statement of power. Since α-particles carry $1/5$ of the total fusion energy per $D+T$ reaction, $Q_\alpha = Q/5$, where Q is the total fusion energy compared to the heating energy supplied [or in the MFE case, stated in terms of total fusion power over heating power, e.g. the goal of ITER[11] is to *reach* $Q \approx 10$ ($Q_\alpha \approx 2$) while the record from the JET tokamak[12] is $Q \approx 0.67$ ($Q_\alpha \approx 0.13$)].

A burning plasma is distinct from other scientific milestones in inertial fusion. Several years prior the first milestone of 'fuel gain'[13] ($G_{fuel} > 1$) was achieved[14], in which the fusion yield exceeds the energy delivered to the fuel; this corresponds to $\sim 12-14$ kJ of yield on NIF. At 20-22kJ, the yield was approximately doubled by self-heating feedback, termed 'alpha heating'[15]. The next scientific milestone is a burning plasma, as described previously; this is the scientific milestone achieved in this work. No *net* energy gain, G, relative to the laser energy is expected for a burning plasma. Because of energy losses incurred in achieving the required compressed state, ICF implosions must achieve ignition before a net energy gain is possible. A net energy gain would require fusion yields greater than the laser energy, 1.9 MJ. While short of ignition or energy gain, a burning plasma ($Q_\alpha > 1$) is a new physics regime for laboratory fusion[1,11,16]. Studying burning plasmas will elucidate other new physics in this regime, such as self-heating driven instabilities or kinetic effects in the plasma, which likely depend on confinement approach.

In a tokamak, the predominant approach to magnetic confinement, once the plasma discharge is generated by resistive heating, external power sources, such as radio-frequency antenna, provide additional plasma heating as the plasma is brought to fusion conditions. In indirect-drive ICF, the way energy is delivered to the fusion fuel is different and much less direct. On the National Ignition Facility (NIF)[17] 192 lasers deliver up to 1.9 MJ of frequency-tripled light into a high atomic number (Z) "hohlraum" (Fig. 1) that serves the purpose of an x-ray converter generating a nearly Planckian x-ray bath, an approach known as 'indirect drive'[18]. The incident beam-by-beam laser pointing and power in time are designed[6] to generate a specific radiation temperature (T_{rad}) history (Fig. 1, lower left) inside the hohlraum with sufficient uniformity in a way that is matched to specifics of the target geometry and desired final plasma state. The exposed surface of a capsule at the center of the hohlraum absorbs $\sim 10-15\%$ of the x rays, causing the outer edge of the capsule (the ablator) to ionize, generate high pressures of order hundreds of Mbar (1 Mbar = 10^{11} Pa), and expand away from the capsule – a process termed ablation. A shell of cryogenic DT fuel is layered against the inside surface of the ablator, which is in partial-pressure equilibrium with DT vapor in the center of the capsule (Fig. 1 upper left). The inwardly-directed acceleration caused by the ablation drives the capsule and DT fuel inwards upon itself (an implosion, shown schematically at the right of Fig. 1) with enormous acceleration ($\sim 10^{13}$ g's) obtaining velocities of $\sim 350-400$ km/s in a matter of nano-seconds. Most of the capsule absorbed x-ray energy ($\sim 92-95\%$) is consumed by the ablation process, but as a result the DT fuel obtains significant ($\sim 10-20$ kJ) kinetic energy (KE) inside a very small volume.

Shortly after the DT fuel acquires peak KE, the pressure (P) inside the implosion rises dramatically, to levels of many hundreds of Gbar (1 Gbar = 10^{14} Pa), as KE is converted into internal energy (IE) in the DT (a process termed stagnation). An ICF implosion is a pressure amplifier, sacrificing absorbed energy to achieve high *energy density* and central pressures that are factors of thousands higher than the pressure at the ablation front. The high central pressure is necessary because only a small fraction of the NIF facility energy can ever be coupled into the DT fuel and heating a large mass of DT fuel is energetically costly, as reflected in the heat capacity of DT, $c_{DT} = 115$ kJ/(mg·keV) [9.9×10^3 J/(kg·K)]. In these experiments the total fuel mass is ~ 200 μg and the hot-spot mass is $\sim 20-30$ μg. Since high ion temperature (T_i) is also needed for fusion, as the fuel stagnates at the center of the implosion, the DT forms a hot-spot from the fuel's inner surface and PdV work is done on the hot-spot generating very high ion and electron temperatures in near thermal equilibrium ($T_i \approx T_e \sim 4-5$ keV, 1 keV = 1.16×10^7 K, where T_i and T_e are the ion and electron temperatures). If the conditions of high temperature and pressure are achieved, the hot-spot initiates copious DT fusion reactions and self-heating further increases T_i.

ICF experiments demonstrated significant fusion performance enhancement from self-heating[14,15] several years ago, and more recent advances[19–21] generated experiments with ~ 50 kJ fusion yields that were close to the burning plasma threshold[3]. These experiments used capsules with similar inner radii, between $0.91-0.95$ mm. Within the maximum laser energy NIF can deliver, these previous designs were limited in the energy coupled to the capsule, and thus in the fuel kinetic energy, by the ability to control the symmetry of the radiation environment within the hohlraum, primarily due to the fact that an ablated plasma bubble expands from where the outer beams hit the wall (see Fig. 1) intercepting the inner beams and thereby suppressing drive at the hohlraum waist[22,23]. Two tactics have been employed to enable symmetry control with more efficient hohlraums driving larger capsules: adjusting cross-beam energy transfer between the outer to inner beams[4,24,25] by changing the laser wavelength separation ($\Delta\lambda$), and incorporating a pocket in the hohlraum wall at the outer beam location to delay the bubble propagation[5]. These tactics have been used to design higher efficiency hohlraums that control symmetry; we use these hohlraums to drive capsules that are $\sim 10\%$ larger than prior experiments to realize the strategy for achieving a burning plasma laid out in Ref. 2. These experimental campaigns are known as 'Hybrid E' and 'I-Raum'; the Hybrid-E campaign uses $\Delta\lambda$ exclusively while I-Raum uses a combination of the pocket and $\Delta\lambda$. Key data and analysis supporting this burning-plasma analysis are given in accompanying papers: by Ross, Ralph, Zylstra, et al. (Ref. 7 on experiments), and by Kritcher, Young, Robey, et al. (Ref. 6 on design simulations).

Four experiments with these new designs have been conducted that have generated record performance on the NIF, with fusion yield tripled from past experiments[4,19,21] to a maximum $\sim$ 170 kJ[26]; the experiments are referred to by a experiment number denoting the date of the experiment (e.g. NYYMMDD, YY=year, MM=month, DD=day format). N201101 and N210207 were experiments using the Hybrid-E platform while N201122 and N210220 were experiments using the I-Raum platform. The experiments in November (N201101 and N201122) achieved much higher performance relative to past work due to their increased scale and favorable implosion design parameters yet each suffered from low-mode degradations; these low-mode asymmetries were mitigated on the subsequent experiments (N210207 and N210220) resulting in higher performance (see Refs. 6, 7).

On each NIF experiment a comprehensive suite of optical, x-ray, and nuclear diagnostics measure key aspects of the implosion performance. Key data are shown in Extended Data Table 1: the total fusion yield in kJ, ion temperature (T_i, measured from DD reactions[7]), hot-spot volume, and burn width in ps. For a full description of the experimental data and changes between the experiments, see Ref. 7. Analytic models, using these data, are used to infer characteristics of the implosion process and hot spot including the pressure, hot-spot internal energy, implosion velocity and peak kinetic energy in the fuel during implosion, PdV work done on the hot spot, and areal density of the hot spot in g/cm^2. These quantities are required to evaluate the burning-plasma criteria. Most of these inferences are described in Ref. 27 and the Methods; the implosion velocity (v_{imp}) can be inferred from the time of maximum neutron output ('bang-time') and an implosion dynamics 'rocket-model' that is calibrated to

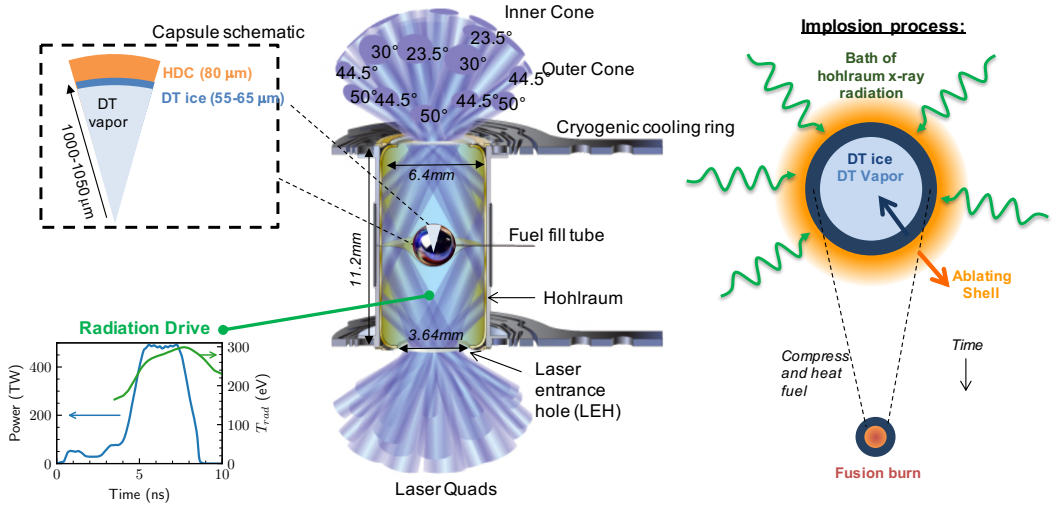

Figure 1: (Center) A typical indirect-drive target configuration with key engineering elements labeled. Laser beams (blue) enter the hohlraum through laser entrance holes at various angles. (Upper left) A schematic pie diagram showing the radial distribution and dimensions of materials in diamond (high density carbon, HDC) ablator implosions. (Lower left) The temporal laser power pulse-shape (blue) and associated hohlraum radiation temperature (green). (Right) At the center of the hohlraum, the capsule is bathed in x-rays, which ablate the outer surface of the capsule. The pressure generated drives the capsule inward upon itself (an implosion) which compresses and heats the fusion fuel during the implosion process.

near-neighbor surrogate experiments where the implosion trajectory is tracked radiographically[28,29].

While it would be desirable to have a direct measure that indicates a burning plasma, such a measurement is not yet known to exist, so inferences from data must be used instead. G_{fuel} has a direct connection to ignited fusion requirements and suggests a simple metric for assessing a burning plasma from $G_{fuel} = Y/E_{PdV,tot}$ where Y is the fusion yield and $E_{PdV,tot}$ is the total PdV work on the fuel (see Methods for how this quantity is evaluated). Fig. 2a (also see Extended Data Table 1) shows a plot of G_{fuel} data from many DT implosions on NIF versus the product $pT^{1.6}\tau$ where τ is a confinement time; this is a Lawson-like criterion applicable for G_{fuel} (see Methods).

As can be seen in Fig. 2a, most experimental series show a linear trend between G_{fuel} and $PT_i^{1.6}\tau$ and have $G_{fuel} \leq 5$. Whereas, the Hybrid-E and I-Raum implosion series show a transition to a super-linear trend between G_{fuel} and $PT_i^{1.6}\tau$ (as expected when self-heating exceeds the hot-spot internal energy) and have $G_{fuel} > 5$. The non-burning plasma regime is denoted by the gray shaded region ($G_{fuel} < 5$). In this and the following figures, historical data from NIF are shown from Refs. 4, 14, 15, 19–21, 31–33, labeled by the names of those predecessor campaigns.

Fig. 2b shows the probable distribution of the G_{fuel} values plotted in Fig. 2a, with the probability distribution in the inferred data quantities included to evaluate the uncertainty (see Methods). For comparison, we include a set of previous high-performing NIF experiments from Refs. 4, 19, 21. The abscissa of Fig. 2b are NIF experiment numbers; while several experiments in years prior to November 2020 came very close to the threshold of $G_{fuel} = 5$, only the experiments reported here have so far clearly surpassed it (see Extended Data Table 1 for values, where the quoted likelihood is the fraction of the distribution above the threshold).

Alternatively, comparing the total energy produced in α-particles, $E_\alpha = Y/5$, to the peak DT fuel KE_{fuel} (see Fig. 2c) is another simple metric. Similar to Fig. 2b, Fig. 2d shows the probable range of E_α/KE_{fuel}, with normally distributed uncertainties in the input data vs. experiment number for the eight highest performing DT experiments on the NIF, where again only these four experiments clearly exceed $E_\alpha/KE_{fuel} > 1$ (see Extended Data Table 1 for values). Since indirect-drive implosions have a small fraction of ablator mass remaining at peak velocity it is important to point out that KE_{fuel} is not the total implosion kinetic energy at peak velocity, but because the stagnating shell is compressible and extended radially, only a fraction of the ablator's kinetic energy can be converted to internal energy before peak burn and disassembly.

While G_{fuel} and E_α/KE_{fuel} are suggestive metrics for an ICF burning plasma, two more rigorous and more stringent metrics already exist in the literature[3,8]. The burning plasma statement that "α-deposition is the dominant source of plasma heating" is complicated by the temporal nature of an implosion, where the PdV work on the hot-spot that does the heating comes before the time of peak fusion-rate, a consideration that is not analogous to MFE. Hurricane et al. published a condition on velocity (v_{cond})[2,3] relative to the plasma conditions, which we slightly modify (see Methods) to:

$$v_{cond}(\rho R_{hs}, T_i) = 5.3 \times 10^{25} (\rho R)_{hs} \frac{\langle \sigma v \rangle}{T_i} > v_{imp} \qquad (1)$$

in units of keV, g, cm, and s. Here, ρR_{hs} is the hot-spot areal density and $\langle \sigma v \rangle$ is the fusion reactivity.

To evaluate the Hurricane metric the hot-spot temperature and areal density, and the implosion velocity are needed (see Methods). The thermonuclear reactivity $\langle \sigma v \rangle$ is a function of the hot spot conditions, specifically the temperature; we use Bosch and Hale's[34] $\langle \sigma v \rangle$ evaluation. Fig. 3a shows the experiments in hot-spot temperature and areal density parameter space. Previous experiments are shown as points, while these two experiments are shown as full probability distributions [red (N201101), blue (N201122), purple (N210207), and grey (N210220)], with contours enclosing 80% of the distribution. In Fig. 3a a single contour of Eq. 1 for $v_{imp} = 385$ km/s, representative of these experiments, is shown. When evaluating the criteria each experiment's actual inferred velocity, with uncertainty, is used. These are the first experiments to exceed the Hurricane criterion, as clearly shown by the probability distributions in Fig. 3b. The likelihood of these four experiments exceeding the criteria is 89% (N201101), 79% (N201122), and 100% for both N210207 and N210220.

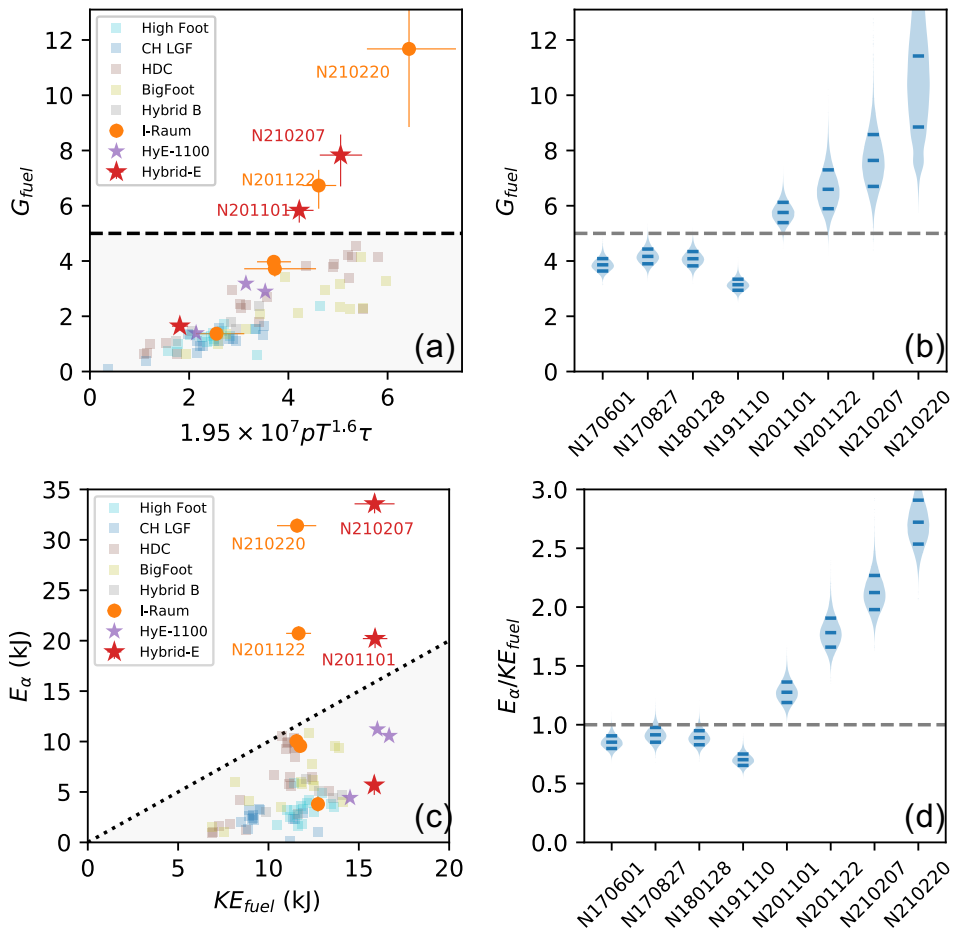

Figure 2: Simple metrics for assessing a burning plasma. (a) total fuel gain versus Lawson-like parameter, $G_{fuel} > 5$ corresponds to the burning plasma regime. (b) Probability distributions for G_{fuel} for high-performing experiments, in these plots the width of the shaded region is proportional to the probability distribution and the solid lines mark the 16, 50, and 84 percentile of the distribution (c) Total alpha-heating energy vs fuel kinetic energy, $E_\alpha/KE_{fuel} > 1$ corresponds to $Q_\alpha > 1$. (d) Probability distributions in E_α/KE_{fuel} criteria for high performing experiments

Eq. 1 should be roughly equivalent to the burning-plasma criteria found by Betti, *et al.* ($3.5\times$ yield amplification and $0.5E_\alpha/E_{PdV,hs} > 1$)[8], but for completeness we use both. The first criteria by Betti *et al.*, $Y_{amp} \geq 3.5$, is satisfied by our inferred yield amplifications given in Extended Data Table 1, inferred with the prescription in Ref. 27 and from 2-D simulations[6] using HYDRA[35]. Two quantities are required to evaluate the second Betti *et al.* burning-plasma metric. The alpha deposited energy (E_α) is straightforward as it is simply 20% of the measured total fusion yield (given in Extended Data Table 1), which is ~ 20 kJ for the first two experiments, ~ 33 kJ for N210207, and ~ 31 kJ for N210220. The second input for this criteria is the PdV work done upon the hot spot, which must be inferred – inferences prone to large uncertainties in the presence of significant α-heating and bremsstrahlung x-ray losses. We perform this inference two ways (see Methods), first using an analytic hydrodynamic piston model[36] of an implosion, and second by extracting PdV work from the 2-D radiation-hydrodynamics simulations that best match the experimental observables as described in Ref. 6. These two estimates are used to estimate a range in hot-spot PdV work and are both plotted in Fig. 3c compared to previous experiments on the NIF, with a $1-1$ line to denote the burning plasma regime (above the line). Probability distributions for the metric quantity itself are shown in Fig. 3d. From Betti's criteria, with the experimental (simulated) $E_{PdV,hs}$ we assess 74% (0%) and 97% (2%) probability, experiments N201101 and N201122, respectively, are in the burning plasma regime. The difference in probability reflects the fact that the simulated PdV work is higher and thus is more pessimistic for satisfying the criteria, with the simulated values for these experiments being below the burning plasma threshold. With improved performance, experiments N210207 and N210220 are assessed to be in the burning plasma regime with 100% confidence by both experimental and simulated methodologies. These correspond to an an inferred $Q_\alpha \sim 1.4-1.6$ for experiment N210207, and $Q_\alpha \sim 1.3-2.0$ for experiment N210220.

Several metrics for assessing whether these implosions created a burning plasma state have been discussed and presented in Extended Data Table 1 and Figures 2 and 3. In each case burning plasma likelihoods are calculated by propagating uncertainties in each quantity through the metric (see Methods), shown in the figures with likelihood values discussed and summarized in Extended Data Table 1. Quantitatively, we see that the first two (N201101 and N201122) are assessed as likely being in the burning plasma regime by all metrics excpt Betti's when evaluated with the simulated $E_{PdV,hs}$; the most recent experiments (N210207 and N210220) are overwhelmingly likely to have passed this threshold. Qualitatively, our confidence in this conclusion is further increased by the use of multiple independent metrics.

The achievement of a burning plasma state is key progress towards the larger goal of 'ignition' and overall energy gain in inertial fusion.

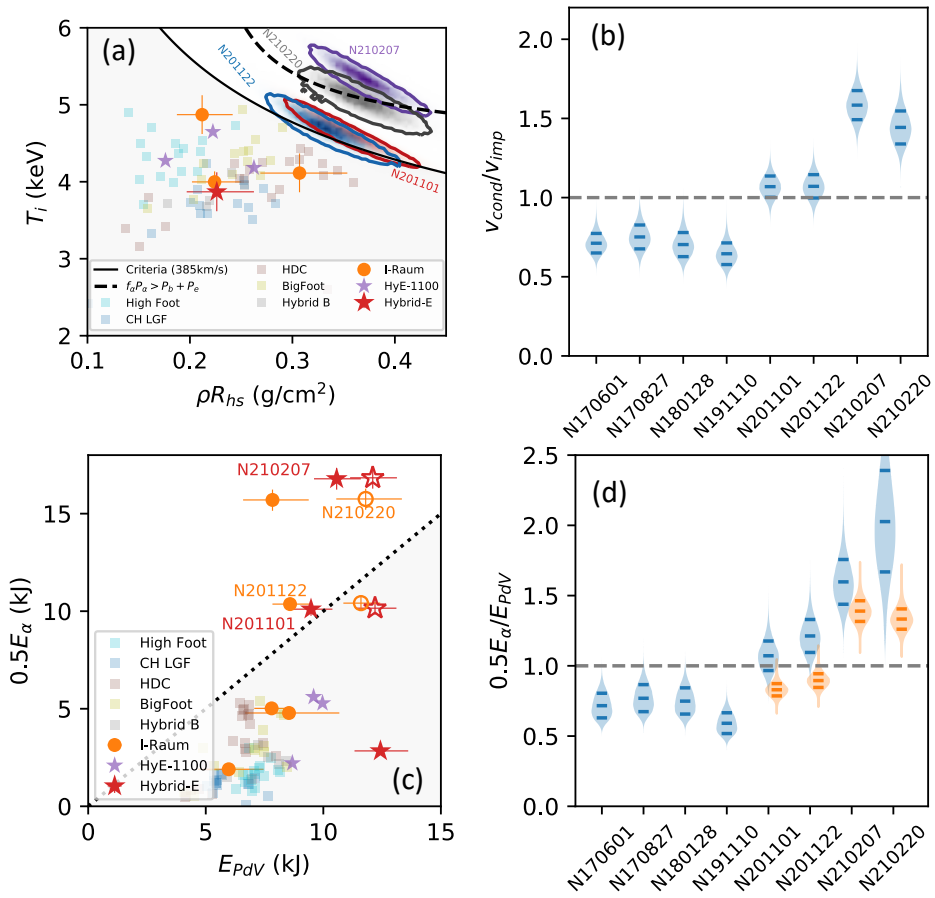

Figure 3: ICF-specific burning plasma metrics. (a) Criteria on temperature and hot-spot ρR established by Hurricane et al. (Ref. 3) (b) probability distribution for experiments exceeding the Hurricane criteria, > 1 is a burning plasma. (c) Criteria on alpha heating and PdV work from Betti et al. (Ref. 8), including estimates from data inferences (solid symbols) and from 2-D simulations (open symbols) (d) probability distribution for experiments exceeding the Betti criteria, for these experiments distributions are shown for data-inferred $E_{PdV,hs}$ (blue) and using 2-D simulations (orange).

The record fusion yields reported here ($\sim$ 0.17 MJ) are lower than the input laser energy ($\sim$ 1.9MJ), but are nearly equal to the capsule absorbed energy (giving capsule gain, $G_{capsule} \sim 0.7 - 0.8$) and are an order of magnitude greater than the input energy transferred to the fusion fuel. Moreover, the total fusion power ($5mP_\alpha$) generated in the two highest performing experiments are at petawatt levels (e.g. $\sim 1.6 \pm 0.2$ PW for N210207).[26]

In the burning plasma regime, self-heating can overtake loss mechanisms, which include bremsstrahlung losses, thermal conductivity, and negative PdV work upon expansion. Simple expressions for the power balance terms are given in the Methods and values for the four experiments are given in Extended Data Table 1. Here, we use a bremsstrahlung enhancement factor $f_b \sim 1.15$ which is inferred from the data[37]. The first two experiments have self-heating comparable to the radiation losses. An important new regime is when self-heating is greater than both the radiation and conduction losses ($f_\alpha P_\alpha > P_b + P_e$), a contour for this regime is shown in Fig. 3a by the black dashed line. Experiment N210220 is close to entering this regime, and we infer that experiment N210207 has entered this regime for the first time with 82% likelihood. The level of alpha heating is still short of that required for ignition[26].

In order to achieve ignition, defined as a yield amplification ($Y_{amp} \sim 20-30$) consistent with ~ 1 MJ fusion yield[38], and then high gain, further progress is needed [26]. Fig. 4 shows these experiments in the larger context of ignition, in the parameter space of hot-spot pressure and energy (a) and in yield amplification versus a Lawson-like parameter called the 'ignition threshold factor' experimentally inferred (ITFX)[18,27,39] for conditions without alpha heating ($n\alpha$, b). Fig. 4b plots this quantity as $ITFX_{n\alpha}^{0.34}$ which is approximately equivalent to $\chi_{n\alpha}$ as defined in Ref. 8. Proximity to ignition can be gauged qualitatively in terms of the product $P^2 E_{hs}$ [equivalent to $(\rho R_{hs} T_i)^3$], or in terms of $ITFX_{n\alpha}$ or $\chi_{n\alpha} \sim 1$ representing ignition. Fig. 4a shows contours of $P^2 E_{hs}$ relative to N210207 showing that this metric has been improved by a factor of several from previous results. From Fig. 4 we clearly see that these four experiments are the closest to ignition, but a further increase in $ITFX_{n\alpha}$ from $\sim 0.6 \rightarrow 1$ is required.

As discussed in the accompanying Articles[6,7], these experiments have clear and specific degradation mechanisms which can be mitigated for further improvement in performance. More generally, the ICF program on NIF is pursuing several approaches that can enable additional progress: reducing degradation mechanisms including low-mode asymmetry[40–42] and radiative losses from mix[37], further increasing energy coupled to the capsule[4,43], and improving compression of the fuel[44].

In conclusion, we have generated, for the first time in the laboratory, a burning plasma state in which the plasma is predominantly self-heated. This was accomplished using inertial fusion implosions on the US National Ignition Facility; previous experiments here were

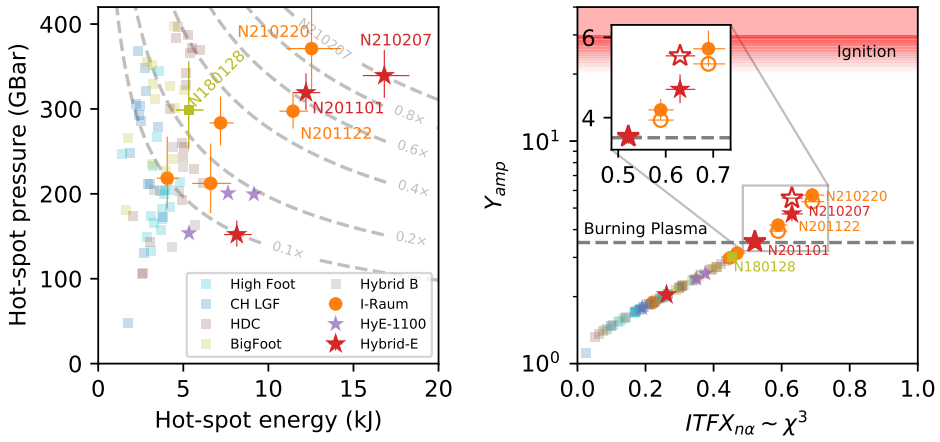

Figure 4: These experiments in parameter space relevant for ignition. Left: Hot-spot pressure and energy. The product $P^2 E_{HS}$ is representative of proximity to ignition, contours of this metric relative to N210207 are shown by the dashed gray curves. Right: Yield amplification (Y_{amp}) versus $ITFX_{n\alpha}$. These are the highest performing ICF experiments to date and the closest to ignition. The inset shows these experiments in detail with both inferred (solid) and simulated (open) Y_{amp}.

just below the threshold for a burning plasma, we increased the capsule scale relative to previous work, increased the coupling efficiency from laser energy to the capsule, and controlled implosion symmetry using new tactics. Four experiments have been conducted that have passed the threshold for a burning plasma by several metrics, with especially high confidence on the most recent two experiments. Additionally, the highest performing experiment (N210207) is in a more stringent regime where the self-heating surpasses energy losses from radiation and conduction. While these results are short of total energy gain from the system due to the inherent inefficiencies of ICF, these experiments represent a substantial step towards this goal with record values of parameters that assess our proximity to ignition on NIF. Several promising avenues for further increases in performance are identified and will be pursued by the US inertial fusion program, in addition to novel physics in the burning-plasma regime such as alpha-driven processes.

1. Mauel, M. *et al. Final Report of the Committee on a Strategic Plan for U.S. Burning Plasma Research* (National Academies Press, Washington, D.C., 2019).
2. Hurricane, O. A. *et al.* Beyond alpha-heating: driving inertially confined fusion implosions toward a burning-plasma state on the National Ignition Facility. *Plasma Physics and Controlled Fusion* **61**, 014033 (2019).
3. Hurricane, O. A. *et al.* Approaching a burning plasma on the NIF. *Phys. Plasmas* **26**, 052704 (2019).
4. Zylstra, A. B. *et al.* Record Energetics for an Inertial Fusion Implosion at NIF. *Phys. Rev. Lett.* **126**, 025001 (2021).
5. Robey, H. F., Berzak Hopkins, L., Milovich, J. L. & Meezan, N. B. The I-Raum: A new shaped hohlraum for improved inner beam propagation in indirectly-driven ICF implosions on the National Ignition Facility. *Phys. Plasmas* **25**, 012711 (2018).
6. Kritcher, A., Young, C., Robey, H. *et al.* Design of inertial fusion implosions reaching the burning plasma regime. *Nature Physics* (2021).
7. Ross, J. S., Ralph, J., Zylstra, A. *et al.* Experiments conducted in the burning plasma regime with inertial fusion implosions. *Nature Physics* (2021).
8. Betti, R. *et al.* Alpha Heating and Burning Plasmas in Inertial Confinement Fusion. *Phys. Rev. Lett.* **114**, 255003 (2015).
9. Lawson, J. D. Some criteria for a power producing thermonuclear reactor. *Proceedings of the Physical Society. Section B* **70**, 6 (1957).
10. Nuckolls, J., Wood, L., Thiessen, A. & Zimmerman, G. Laser Compression of Matter to Super-High Densities: Thermonuclear (CTR) Applications. *Nature* **239**, 139–142 (1972).
11. Green, B. *et al.* ITER: burning plasma physics experiment. *Plasma Physics and Controlled Fusion* **45**, 687 (2003).
12. Keilhacker, M. *et al.* High fusion performance from deuterium-tritium plasmas in JET. *Nuclear Fusion* **39**, 209–234 (1999).
13. Atzeni, S. & Meyer-Ter-Vehn, J. *The Physics of Inertial Fusion* (Oxford University Press, Oxford, Great Britain, 2004).
14. Hurricane, O. *et al.* Fuel gain exceeding unity in an inertially confined fusion implosion. *Nature* **506**, 343 (2014).
15. Hurricane, O. A. *et al.* Inertially confined fusion plasmas dominated by alpha-particle self-heating. *Nature Physics* **12**, 800 (2016).
16. Coppi, B. Evolving Developments for the Scientific Community and for Controlled Nuclear Fusion and Space Research. In B.L. Altshuler, M.A. Vasiliev, L.I. Gurvits, I.M. Dremin, V.I. Ritus, V.E. Fortov, A.E. Shabad (ed.) *Academician A.D. Sakharov. Scientific Works. To His Centenary*, vol. 1 of *Journal of Physics Conference Series* (Fizmatlit Publ., Moscow, 2021, 2021). MIT (LNS) Report HEP 20/03 (2020) to be published in Russian.
17. Moses, E. I. *et al.* The National Ignition Facility: Transition to a User Facility. *Journal of Physics: Conference Series* **688**, 012073 (2016).
18. Lindl, J. Development of the indirect-drive approach to inertial confinement fusion and the target physics basis for ignition and gain. *Phys. Plasmas* **2**, 3933–4024 (1995).
19. Le Pape, S. *et al.* Fusion Energy Output Greater than the Kinetic Energy of an Imploding Shell at the National Ignition Facility. *Phys. Rev. Lett.* **120**, 245003 (2018).
20. Casey, D. T. *et al.* The high velocity, high adiabat, "Bigfoot" campaign and tests of indirect-drive implosion scaling. *Phys. Plasmas* **25**, 056308 (2018).
21. Baker, K. L. *et al.* Hotspot parameter scaling with velocity and yield for high-adiabat layered implosions at the National Ignition Facility. *Phys. Rev. E* **102**, 023210 (2020).
22. Callahan, D. A. *et al.* Exploring the limits of case-to-capsule ratio, pulse length, and picket energy for symmetric hohlraum drive on the National Ignition Facility Laser. *Phys. Plasmas* **25**, 056305 (2018).
23. Hopkins, L. B. *et al.* Toward a burning plasma state using diamond ablator inertially confined fusion (ICF) implosions on the national ignition facility (NIF). *Plasma Physics and Controlled Fusion* **61**, 014023 (2018).
24. Michel, P. *et al.* Symmetry tuning via controlled crossed-beam energy transfer on the National Ignition Facility. *Phys. Plasmas* **17**, 056305 (2010).
25. Glenzer, S. H. *et al.* Symmetric inertial confinement fusion implosions at ultra-high laser energies. *Science* **327**, 1228–1231 (2010).
26. As this paper was being finalized, a new experiment in this series on august 8, 2021 produced $\sim$ 1.35 mj of fusion yield and $g_{capsule} \sim 5$ breaking all previous records and was subject to a press release https://www.llnl.gov/news/national-ignition-facility-experiment-puts-researchers-threshold-fusion-ignition. this new experiment built upon the experiments of this manuscript, but is not documented here.
27. Patel, P. K. *et al.* Hotspot conditions achieved in inertial confinement fusion experiments on the National Ignition Facility. *Phys. Plasmas* **27**, 050901 (2020).
28. Landen, O. L. *et al.* Capsule implosion optimization during the indirect-drive National Ignition Campaign. *Phys. Plasmas* **18**, 051002 (2011).

29. Meezan, N. B. *et al.* X-ray driven implosions at ignition relevant velocities on the National Ignition Facility. *Phys. Plasmas* **20**, 056311 (2013).
30. Hurricane, O. *et al.* Physics Principles of Inertial Confinement Fusion (ICF) and Status of the US Program. *Reviews of Modern Physics* **in preparation**, 58 (2021).
31. Baker, K. L. *et al.* High-performance indirect-drive cryogenic implosions at high adiabat on the national ignition facility. *Phys. Rev. Lett.* **121**, 135001 (2018).
32. Döppner, T. *et al.* Achieving 280 gbar hot spot pressure in dt-layered ch capsule implosions at the national ignition facility. *Phys. Plasmas* **27**, 042701 (2020).
33. Hohenberger, M. *et al.* Integrated performance of large hdc-capsule implosions on the national ignition facility. *Phys. Plasmas* **27**, 112704 (2020).
34. Bosch, H.-S. & Hale, G. Improved formulas for fusion cross-sections and thermal reactivities. *Nuclear Fusion* **32**, 611–631 (1992).
35. Marinak, M. M. *et al.* Three-dimensional hydra simulations of national ignition facility targets. *Phys. Plasmas* **8**, 2275–2280 (2001).
36. Hurricane, O. A. *et al.* An analytic asymmetric-piston model for the impact of mode-1 shell asymmetry on ICF implosions. *Phys. Plasmas* **27**, 062704 (2020).
37. Pak, A. *et al.* Impact of Localized Radiative Loss on Inertial Confinement Fusion Implosions. *Phys. Rev. Lett.* **124**, 145001 (2020).
38. Christopherson, A. R., Betti, R. & Lindl, J. D. Thermonuclear ignition and the onset of propagating burn in inertial fusion implosions. *Phys. Rev. E* **99**, 021201 (2019).
39. Spears, B. K. *et al.* Performance metrics for inertial confinement fusion implosions: Aspects of the technical framework for measuring progress in the National Ignition Campaign. *Phys. Plasmas* **19**, 056316 (2012).
40. Rinderknecht, H. G. *et al.* Azimuthal Drive Asymmetry in Inertial Confinement Fusion Implosions on the National Ignition Facility. *Phys. Rev. Lett.* **124**, 145002 (2020).
41. Tommasini, R. *et al.* Time-Resolved Fuel Density Profiles of the Stagnation Phase of Indirect-Drive Inertial Confinement Implosions. *Phys. Rev. Lett.* **125**, 155003 (2020).
42. Casey, D. T. *et al.* Evidence of Three-Dimensional Asymmetries Seeded by High-Density Carbon-Ablator Nonuniformity in Experiments at the National Ignition Facility. *Phys. Rev. Lett.* **126**, 025002 (2021).
43. Amendt, P. *et al.* Ultra-high ($> 30\%$) coupling efficiency designs for demonstrating central hot-spot ignition on the National Ignition Facility using a Frustraum. *Phys. Plasmas* **26**, 082707 (2019).
44. Landen, O. *et al.* Yield and compression trends and reproducibility at NIF*. *High Energy Density Physics* **36**, 100755 (2020).
45. Cerjan, C., Springer, P. T. & Sepke, S. M. Integrated diagnostic analysis of inertial confinement fusion capsule performance. *Phys. Plasmas* **20**, 056319 (2013).
46. Hurricane, O. A. *et al.* On the importance of minimizing "coast-time" in x-ray driven inertially confined fusion implosions. *Phys. Plasmas* **24**, 092706 (2017).
47. Albright, B. *et al.* Comment on the burning plasma condition of Hurricane et. al [Phys. Plasmas 26, 052704, 2019] and implications for the experimental achievement of a burning plasma state on the NIF. *LA-UR-21-25149* (2021).
48. de Souza, R. S., Boston, S. R., Coc, A. & Iliadis, C. Thermonuclear fusion rates for tritium + deuterium using Bayesian methods. *Phys. Rev. C* **99**, 014619 (2019).
49. Zylstra, A. B. & Hurricane, O. A. On alpha-particle transport in inertial fusion. *Phys. Plasmas* **26**, 062701 (2019).
50. Abadi, M. *et al.* Tensorflow: A system for large-scale machine learning. In *12th {USENIX} symposium on operating systems design and implementation ({OSDI} 16)*, 265–283 (2016).

Acknowledgements and Disclaimer We thank Bruno Coppi (MIT), Steven C. Cowley (PPPL), Dennis Whyte (MIT), Jim Hammer (LLNL), Mike Farrell (GA), and John Kline (LANL) for thoughtful discussions. The contributions of NIF operations and target fabrication teams to the success of these experiments are gratefully acknowledged. This work was performed under the auspices of the U.S. Department of Energy by Lawrence Livermore National Laboratory under Contract DE-AC52-07NA27344. This document was prepared as an account of work sponsored by an agency of the United States government. Neither the United States government nor Lawrence Livermore National Security, LLC, nor any of their employees makes any warranty, expressed or implied, or assumes any legal liability or responsibility for the accuracy, completeness, or usefulness of any information, apparatus, product, or process disclosed, or represents that its use would not infringe privately owned rights. Reference herein to any specific commercial product, process, or service by trade name, trademark, manufacturer, or otherwise does not necessarily constitute or imply its endorsement, recommendation, or favoring by the United States government or Lawrence Livermore National Security, LLC. The views and opinions of authors expressed herein do not necessarily state or reflect those of the United States government or Lawrence Livermore National Security, LLC, and shall not be used for advertising or product endorsement purposes. LLNL-JRNL-819741-DRAFT

Author Contributions

A.B.Z. hot-spot analysis lead, Hybrid-E experimental lead, wrote sections of the paper; O.A.H. capsule scale/burning plasma strategy, theory, 0D hot-spot models, and wrote sections of paper; D.A.C. empirical hohlraum P_2 model and hohlraum strategy; A.L.K. Hybrid-E design lead, integrated hohlraum group lead; J.E.R. N201101 & N210207 experimentalist and "Shot RI" (shot responsible individual); H.F.R. original I-Raum design lead; J.S.R. I-Raum experimental lead and N201122 Shot RI; C.V.Y. present I-Raum design lead, wrote sections of paper; K.L.B. Hybrid Shot RI; D.T.C. Hybrid Shot RI; T.D. Hybrid Shot RI; L.D. 3D hot-spot analysis; M.H. Hybrid Shot RI; S.L.P. Hybrid Shot RI; A.P. Hybrid & I-Raum Shot RI, physics of capsule engineering defects; P.K.P. 1D hot-spot analysis, Y_{amp} and GLC inference; R.T. Hybrid Shot RI; S.J.A. capsule microstructure physics; P.A.A. hohlraum physics; L.J.A. engineering and targets; B.B. penumbral x-ray diagnostic; D.B. computational physics; L.R.B. x-ray framing camera; L.B.H. HDC design and campaign lead; R.B. ICF physics/ignition theory; S.D.B. cryo layering; R.M.B. RTNAD nuclear diagnostic; N.W.B. neutron diagnostics; E.J.B. project engineering; D.K.B. diagnostics; T.B. capsule fab & metrology; T.M.B. cryo layering; M.W.B. project engineering; P.M.C. DT EOS measurements; B.C. HYDRA code development; T.C. LPI physics; H.C. GLEH x-ray diagnostic; C.C. target fab planning; A.R.C. ignition theory; D.S.C. capsule/instability physics; J.W.C. capsule fabrication; E.L.D. experiments; T.R.D. capsule physics; M.J.E. program management; W.A.F. hohlraum physics; J.E.F. 2DConA image analysis; D.F. nuclear diagnostics; J.F. magnetic recoil spectrometer nuclear diagnostic; J.G. ensemble simulations; M.G.J. magnetic recoil spectrometer diagnostic; S.H.G. ICF physics; G.P.G. nuclear diagnostics; S.H. capsule physics, iPOM analysis; K.D.H. neutron diagnostics; G.N.H. experiments; B.A.H. capsule physics; J.H. computational physics; E.H. nuclear time-of-flight diagnostics; J.E.H. MOR and PAM stability, SSD improvements, and FC control; V.J.H. MOR and PAM stability, SSD improvements, and FC control; H.H. gamma diagnostics; M.C.H. program management; D.E.H. hohlraum physics, CBET studies in Hybrid-C; D.D.H. capsule physics; J.P.H. x-ray diagnostics; W.W.H. management; H.H. capsule fabrication; K.D.H. ensemble simulations; N.I. x-ray diagnostics; L.J. x-ray diagnostics; J.J. neutron diagnostics; O.J. hohlraum physics; G.D.K. HYDRA code development; S.M.K. neutron diagnostics; S.F.K. x-ray diagnostics and analysis; J.K. diagnostic management; Y.K. gamma diagnostics; H.G.K. gamma diagnostics; V.G.K. neutron diagnostics; C.K. capsules; J.M.K. HYDRA code development; J.J.K. targets; O.L.L. velocity analysis; S.L. laser plasma instability (PF3D) code development; D.L. NIF facility management; N.C.L. optical diagnostics; J.D.L. ICF physics; T.M. ICF physics; M.J.M. x-ray diagnostics; B.J.M. mode-1 analysis, backscatter; A.J.M. diagnostic management; S.A.M. integrated design physics; A.G.M. x-ray diagnostics; M.M.M. HYDRA code development lead; D.A.M. x-ray diagnostics; E.V.M. x-ray diagnostics; L.M. capsule physics; K.M. gamma diagnostics; N.B.M. hohlraum physics; P.A.M. LPI physics; M.M. optical diagnostics; J.L.M. hohlraum physics; J.D.M. hohlraum physics; A.S.M. neutron diagnostics; J.W.M. hohlraum physics; T.M. neutron and gamma diagnostics; K.N. project engineering; J.G.D.N. MOR and

PAM stability, SSD improvements, and FC control; A.N. target fab engineering, capsule, and fab planning; R.N. ensembles simulations; M.V.P. HYDRA code development; L.J.P. MOR and PAM stability, SSD improvements, and FC control; J.L.P. ensembles simulations; Y.P. hohlraum physics; B.B.P. hohlraum physics; M.R. capsule fabrication; N.G.R. capsule fabrication; H.R. RTNAD mode-1 analysis; M.R. hohlraum physics; M.S.R. x-ray diagnostics; J.D.S. hohlraum physics; J.S. mode-1 analysis; S.S. capsules; D.J.S. neutron diagnostics; M.B.S. hohlraum diagnostics; C.R.S. HYDRA code development; H.A.S. NLTE opacities (Cretin) code development; S.M.S. HYDRA code development; K.S. mode-1 metrology; M.W.S. kinetic physics; S.S. sagometer data & particle analysis; V.A.S. capsule physics; B.K.S. ensemble simulations; P.T.S. dynamic model, ignition theory; M.S. capsules; S.S. x-ray diagnostics; D.J.S. hohlraum/LPI physics; L.J.S. hohlraum physics; C.A.T. Bigfoot design physics; R.P.J.T. program management; E.R.T. optical diagnostics; P.L.V. neutron imaging diagnostics; C.R.W. capsule/instability physics; K.W. x-ray diagnostics; C.W. capsule fabrication; C.H.W. neutron diagnostics; B.M.V.W. NIF operations lead; D.T.W. hohlraum physics; B.N.W. project engineering; M.Y. capsule fabrication; S.T.Y. MOR and PAM stability, SSD improvements, and FC control; G.B.Z. computational physics lead.

Competing Interests The authors declare that they have no competing financial interests.

Correspondence Correspondence and requests for materials should be addressed to O.A.H. and A.B.Z. (emails: hurricane1@llnl.gov, zylstra1@llnl.gov).

Extended Data Table 1: Data, inferred metrics, and burning-plasma criteria for these four experiments. Percentages indicate probabilities. For the criteria > 1 corresponds to a burning plasma except the first two, with the threshold given in brackets. Error bars formal $\pm 1\sigma$ standard deviations.

		N201101 (Hybrid-E)	N201122 (I-Raum)	N210207 (Hybrid-E)	N210220 (I-Raum)
Laser	Peak Power (TW)	490	485	470	480
	Energy (MJ)	1.89	1.82	1.93	1.78
Data	Yield (kJ)	98.4 ± 2.7	106.2 ± 3.2	170.9 ± 4.8	160.6 ± 4.3
	T_i (keV)	4.61 ± 0.14	4.65 ± 0.14	5.23 ± 0.16	5.13 ± 0.24
	Volume ($10^5 \mu$m^3)	2.5 ± 0.2	2.5 ± 0.2	3.3 ± 0.3	2.2 ± 0.5
	Burn Width (ps)	118 ± 6	137 ± 10	107 ± 13	135 ± 9
Inferred	Pressure (GBar)	319^{+23}_{-21}	297^{+23}_{-20}	339^{+30}_{-26}	371^{+54}_{-48}
	Hot-spot energy (kJ)	$12.2^{+0.9}_{-0.8}$	$11.5^{+0.9}_{-0.8}$	$16.8^{+1.5}_{-1.3}$	$12.5^{+1.8}_{-1.5}$
	Fuel K.E. (kJ)	15.9 ± 1.0	11.6 ± 0.87	15.9 ± 1.0	11.6 ± 0.7
	PdV work (kJ, exp.)	9.5 ± 0.9	8.6 ± 0.8	10.6 ± 1.0	8.0 ± 1.5
	PdV work (kJ, sim.)	12.2 ± 0.5	11.6 ± 0.5	12.1 ± 0.5	11.8 ± 0.5
	Hot-spot ρR (g/cm^2)	$0.36^{+0.04}_{-0.03}$	$0.33^{+0.04}_{-0.03}$	$0.36^{+0.04}_{-0.03}$	$0.36^{+0.04}_{-0.04}$
Criteria	Y_{amp} (exp.) [> 3.5]	3.5 ± 0.2	4.2 ± 0.3	4.7 ± 0.3	5.7 ± 0.5
	Y_{amp} (sim.) [> 3.5]	3.53	3.94	5.54	5.34
	G_{fuel} [> 5]	$5.8^{+0.3}_{-0.4}$ (98.7%)	$6.7^{+0.6}_{-0.8}$ (99.5%)	$7.8^{+0.7}_{-1.0}$ (99.9%)	$11.7^{+2.0}_{-2.4}$ (100%)
	E_α / KE_{fuel}	1.28 ± 0.09 (100%)	1.78 ± 0.13 (100%)	2.12 ± 0.15 (100%)	2.72 ± 0.19 (100%)
	v_{cond}/v_{imp} (Hurricane)	1.08 ± 0.07 (89%)	1.06 ± 0.07 (79%)	1.55 ± 0.13 (100%)	1.43 ± 0.11 (100%)
	$0.5E_\alpha / E_{PdV,hs}$ (Betti, exp.)	1.07 ± 0.11 (74%)	1.21 ± 0.12 (97%)	1.59 ± 0.16 (100%)	2.00 ± 0.36 (100%)
	$0.5E_\alpha / E_{PdV,hs}$ (Betti, sim.)	0.83 ± 0.04 (0%)	0.90 ± 0.05 (2%)	1.39 ± 0.07 (100%)	1.33 ± 0.07 (100%)
Ave. Power	$f_\alpha m P_\alpha$ (TW)	138^{+10}_{-10}	119^{+13}_{-11}	241^{+40}_{-31}	184^{+18}_{-17}
	$m f_b P_b$ (TW)	159^{+33}_{-26}	137^{+29}_{-23}	190^{+41}_{-32}	166^{+31}_{-27}
	$m P_e$ (TW)	20^{+4}_{-4}	21^{+4}_{-4}	36^{+6}_{-6}	26^{+6}_{-5}
	Prob. $f_\alpha P_\alpha > P_b + P_e$	0%	0%	82%	25%

1 Methods

Terminology Definitions of commonly-used mathematical symbols are summarized in Table 2.

Methods Table 2: Definitions for symbols used in this paper.

Symbol	Definition
Q_α	Alpha heating divided by external heating of the fuel, $Q_\alpha > 1$ is a burning plasma.
Q	Total fusion energy divided by external heating energy, $Q > 1$ corresponds to fuel gain.
G	Overall target gain
G_fuel	Fuel gain, equivalent to Q in the ICF context.
$T_{e,i}$	Electron (e) and ion (i) temperature in the fuel
E_{hs}	Energy in the hot spot
KE_{fuel}	Kinetic energy of the imploding fuel
$E_{PdV,hs}$	PdV work done on the hot spot
$E_{PdV,tot}$	PdV work done on all of the fuel
E_α	Energy in all of the alpha particles $1/5$ of the yield
v_{imp}	Implosion velocity of the fuel
Y_{amp}	Yield amplification, i.e. the multiplicative increase in yield due to the fusion self-heating

Reproducibility Experiments subsequent to the ones described in this paper have demonstrated the reproducibility of a burning-plasma state on the NIF, with two additional experiments that have performance comparable to the highest-performing experiments in this paper. These newer experiments, N210307 and N210605, were conducted in the Hybrid E platform. N210307 repeated N210207 albeit using a capsule from a different fabrication batch and produced a yield ~ 145 kJ with an experimentally-inferred $Q_\alpha = 1.34 \pm 0.07$ from the Hurricane criteria. Experiment N210605 reduced the ice layer thickness relative to N210207 and resulted in a lower yield (135 kJ) but high ion temperature with $Q_\alpha = 1.40 \pm 0.10$, again from the Hurricane criteria. This additional experiments confirm that the burning-plasma state is reproducible on NIF, full details and analysis on them will be presented in future publications.

Inferred hot-spot conditions Hot-spot conditions must be inferred from measured quantities using a model. The simplest hot-spot model is to assume an isobaric volume of uniform conditions, as used in Ref. 14 between Eq. 2 and 3, in which case the hot spot number density is given by

$$n = 1.2 \times 10^6 \sqrt{\frac{Y}{\langle\sigma v\rangle V_{hs}\tau}} \tag{2}$$

where Y is the fusion yield in J, $\langle\sigma v\rangle$ is the fusion reactivity which depends on the ion temperature (T_i), V_{hs} is the hot-spot volume in cm^3, and τ is the burn duration in s, for equimolar DT mixtures. The remaining hot-spot quantities follow from the inferred density, including the pressure ($P = (1+Z)nk_BT_i$ with Boltzmann's constant), hot-spot energy ($E_{hs} = 1.5PV_{hs}$), and areal density $\left(\rho R = (2.5n/N_a)\sqrt[3]{3V_{hs}/4\pi}\right)$.

A more detailed inference is to use a one-dimensional profile in radius for temperature and density, maintaining the isobaric assumption. A conduction-limited profile follows the expression[45],

$$T(r) = T_{min} + (T_0 - T_{min})\left[1 - \left(\frac{r}{R_0}\right)^2\right]^{\frac{1}{1+\beta}}, \tag{3}$$

where T_{min} is the temperature at the boundary, T_0 is the central temperature, and R_0 is the hot-spot boundary. β is the thermal conductivity power law, 2.5 from classical Spitzer conductivity. Following Ref. 27 we use a lower value $\beta = 2/3$ which accounts for additional physics, dynamical processes, and reproduces radiation-hydrodynamics simulations. The density profile is then determined by the isobaric assumption through $P \propto nT$ being constant. T_{min} is taken as 1 keV leaving T_0, R_0, and P as free parameters in the model; the data are compared to synthetic data calculated from this 1-D profile with the model parameters adjusted to minimize residuals. As in the 0-D model, the hot-spot energy simply follows from pressure and volume while the areal density is the mass density integrated over the inferred radial profile.

In either dimensionality the model's radius is matched to the experimental measurements, which take a contour of emission level, by calculating synthetic emission images to calculate an equivalent contour radius. The measurements include 2- and 3-D asymmetries, so an equivalent spherical volume, and radius, are calculated using the modal decompositions, where the emission contour measured from the equator (R_{eq}) and pole (R_{po}) are

$$R_{eq} = P_0\left\{1 + \sum_\ell \delta P_\ell \times P_\ell(\cos\theta)\right\} \tag{4}$$

$$R_{po} = M_0\left\{1 + \sum_m \delta M_m \times \cos(m[\phi - \phi_i])\right\} \tag{5}$$

$$R_{hs} = \frac{R_{eq}R_{po}}{M_0} \tag{6}$$

where P_0 and M_0 are the average measured sizes from each view, δP_ℓ (δM_m) is the relative modal amplitude, often referred to as P_ℓ/P_0 with the nomenclature above chosen for clarity. P_ℓ are the Legendre polynomials, and ϕ_m are the orientation of the azimuthal modes. R_{hs} is the hot-spot radius as a function of both θ and ϕ, which is integrated to obtain the volume. Here, the dominant parameters are P_0, M_0, and δP_2 which are given in Ref. 7.

Implosion velocity (v_{imp}) is inferred using a rocket model of the implosion[46] constrained by both supporting experiments, especially in-flight radiography, and the measured time of peak nuclear production on each experiment. The inferred yield amplification given in Extended Data Table 1 is a function of the measured yield, shell compression, and fuel mass (m_{fuel}); both the velocity and Y_{amp} inferences use the prescription given in Ref. 27. The fuel kinetic energy then follows from $\frac{1}{2}m_{fuel}v_{imp}^2$. Our techniques for inferring the PdV work done on the fuel are discussed in the following section.

A comparison of inferred values using 0-D and 1-D models are shown in Table 3. Inferred pressures are highly consistent between these calculations, while hot-spot energies and areal densities are higher in the 1-D model due to significant mass near the 1keV temperature cutoff.

Inferring G_{fuel} Since, from the total fusion yield produced by a mass (m) of DT, over a characteristic confinement-time, τ, is $Y \sim 5mP_\alpha\tau$ ($P_\alpha = 8.2\times10^{24}\rho\langle\sigma v\rangle$ in GJ/(g·s) being the specific DT fusion power for a given mass density, ρ, of DT with reaction-rate $\langle\sigma v\rangle$) and since the internal energy in that DT is $E_{hs} = c_{DT}mT_i$, one can write[30]

$$G_{fuel} = \frac{Y}{E_{PdV,tot}} \approx \frac{\frac{Y}{E_{hs}}}{1 + \frac{E_{fuel}}{E_{hs}} - \frac{q}{10}\frac{Y}{E_{hs}}} \tag{7}$$

$$\text{with } \frac{Y}{E_{hs}} \approx 4.6\times10^{26}P\frac{\langle\sigma v\rangle}{T^2}\tau \tag{8}$$

where P is in Gbars, T_i in keV, and τ in s units. In Eq. 7, the total energy delivered by PdV work, $E_{PdV,tot}$, is determined from the hot-spot and compressed, but cold, DT fuel energy at stagnation, E_{hs} and E_{fuel}, respectively at peak compression. The last term in the denominator represents a correction for additional energy retained by self-heating of the fuel from alpha-particle deposition but not then lost as

Methods Table 3: Comparison of inferred quantities from 0-D and 1-D hot-spot models.

	N201101		N201122		N210207		N210220	
	0-D	1-D	0-D	1-D	0-D	1-D	0-D	1-D
P (GBar)	319^{+23}_{-21}	287^{+20}_{-18}	297^{+23}_{-20}	267^{+20}_{-18}	339^{30}_{-26}	310^{+27}_{-23}	371^{+54}_{-48}	337^{+43}_{-36}
E_{hs} (kJ)	$12.2^{+0.8}_{-0.8}$	$16.8^{+1.3}_{-1.2}$	$11.5^{+0.9}_{-0.8}$	$15.7^{+1.3}_{-1.1}$	$16.8^{+1.5}_{-1.3}$	$23.0^{+2.1}_{-1.8}$	$12.5^{+1.8}_{-1.5}$	$16.9^{+2.3}_{-2.1}$
ρR_{hs} (g/cm^2)	$0.36^{+0.04}_{-0.03}$	$0.36^{+0.04}_{-0.03}$	$0.33^{+0.04}_{-0.03}$	$0.34^{+0.04}_{-0.03}$	$0.36^{+0.04}_{-0.03}$	$0.37^{+0.04}_{-0.04}$	$0.36^{+0.04}_{-0.04}$	$0.37^{+0.04}_{-0.04}$

bremsstrahlung. So, $E_{PdV,tot} \approx E_{hs} + E_{fuel} - qY/10$, where q is a "quality" factor, $0 \leq q \leq 1$, measuring the ability of the implosion to retain self-heating energy[30]. Here we use $q \sim 0.7$, inferred from simulations, and the factor of 10 results from $1/5$ of the fusion energy released as alpha particles and half of those produced up until the time of peak fusion burn. Albeit generally arrived at in a different fashion than above, the product $P(\langle\sigma v\rangle/T^2)\tau$ is Lawson's[9] parameter for ignition. Fig. 2a uses the useful reaction-rate approximation $\langle\sigma v\rangle \approx 4.2 \times 10^{-20} T_i^{3.6}$ (in units of cm^3/s for ion temperature range $3.5 < T_i < 6.5$ keV) to simplify the abscissa.

An expression for the fuel gain is given in Eq. 7. The yield is measured and the hot-spot energy is inferred as described in the prior section. Precisely determining the cold-fuel energy from data is not straightforward. For the purposes of this analysis we actually require the total PdV work done on all the DT. This is at a minimum the fuel kinetic energy and internal energy at peak velocity, which are both inferred. This neglects any work done by the inflowing remaining ablator material on the fuel on the fuel, which can occur in these implosions. In this case the hot-spot energy is more than half the previous estimate; in this scenario we assume equipartition between the hot spot and cold fuel to evaluate Eq. 7.

Inferred PdV work The primary uncertainty in the Betti metric[8] is in the inference of PdV work on the hot spot, here we use three methodologies: two inferences using an analytic model, and a direct extraction of PdV work from simulations that match the experimental observables.

We use the hydrodynamic piston model of an implosion described in Ref. 36. This analytic model abstracts the implosion process using opposed pistons to represent the imploding shell. In spherical geometry, the stagnation pressure from this mechanical work on the hot spot is given by (Eq. 24 in Ref. 36):

$$P_{piston} = \frac{\rho\delta R_{ave}\, v_{imp}^2}{R_{hs}}(1 - f^2), \tag{9}$$

where $\rho\delta R_{ave}$ is the average shell areal density, calculated from the measured neutron 'down scattered ratio' (DSR) using the relation $\rho\delta R_{ave} \sim 19.3 DSR$, v_{imp} is the implosion velocity, and R_{hs} is the average hot spot radius (which can be obtained from the volume, V_{hs}, given in Extended Data Table 1). The factor f^2 represents the effect of mode-1 asymmetry and is a measure of the residual kinetic energy (kinetic energy that is never converted into internal energy) in the implosion.

From the piston pressure we obtain the hot-spot internal energy (E_{hs}) from

$$E_{hs} = \frac{3}{2} P_{piston} V_{hs}. \tag{10}$$

In the absence of α-heating (which adds energy to the hot-spot) and radiative x-ray losses, or when α-heating exactly balances x-ray losses, then $E_{hs} = E_{PdV,hs}$. For low yield amplification implosions ($Y_{amp} < 1.5$), x-ray losses dominate over α-heating energy gains, so $E_{hs} < E_{PdV,hs}$. For higher yield amplification implosions ($Y_{amp} > 2$), α-heating energy gains start to dominate over x-ray losses, so $E_{hs} > E_{PdV,hs}$. The estimated values for these four experiments are given in Table 4 as the piston methodology.

Methods Table 4: Inferred hot-spot PdV work by different methodologies, ordered from smallest to largest estimates.

		N201101	N201122	N210207	N210220
Data	Stag. Mass	9.5 ± 1.1	7.0 ± 0.8	9.5 ± 1.1	6.9 ± 0.8
	Piston	9.5 ± 0.9	8.6 ± 0.8	10.6 ± 1.0	8.0 ± 1.5
Sim.	2-D ($\pm$0.5)	11.5	13.4	12.1	11.8
	1-D	11.3	10.4	11.1	10.5

We can also estimate the stagnated fuel mass in a similar fashion using

$$m_{shell} = 4\pi R_{hs}^2 \rho\delta R_{ave}, \tag{11}$$

which allows us to then estimate the total mass that stagnates from $m_{shell} + m_{hs}$, with m_{hs} from the hot-spot inferences described earlier. We then estimate the PdV work from

$$E_{PdV,hs} = 0.73 K E_{fuel} \frac{m_{shell} + m_{hs}}{m_{fuel}}, \tag{12}$$

where m_{fuel} is the initial fuel mass. The factor of 0.73 is derived from 1-D simulations in which the imploding mass stagnates efficiently, and we drop the residual kinetic energy factor f^2 since the inferred shell mass does not include non-stagnated material. This estimate leads to smaller estimates of $E_{PdV,hs}$ than the first empirical estimate, and are given in Table 4 as the stagnated mass estimate.

For analysis of previously published campaigns we use the simple relation $E_{PdV,hs} \sim (0.5{-}0.7) K E_{fuel}(1{-}f^2)$, this is easy to evaluate with the available data and the factor $0.5{-}0.7$ accounts for a wide range of 1-D to 2-D/3-D behavior observed on past experiments. For comparison, the proportionality constant inferred from the first methodology (Eq. 10) is between 0.60 and 0.73 for our four experiments.

We also employ radiation-hydrodynamics simulations to estimate the PdV work done on these implosions. The first simulation-based methodology is to use 2-D simulations with degradation mechanisms that match the observed performance, and interrogate the work done upon the mass elements which form the hot spot to infer $E_{PdV,hs}$. The simulation methodology is described in Ref. 6, and the values of $E_{PdV,hs}$ for this method are given in Table 4. The same fusion performance can be generated with varying application of degradation mechanisms that either degrade $E_{PdV,hs}$ or do not; an estimate of the 2-D simulation uncertainty of ± 0.5 kJ is estimated by studying multiple simulations.

A similar energy-balance analysis can be done with 1-D simulations, in which the work done upon the hot spot is well defined with a Lagrangian mesh. The 1-D simulations are tuned to match the measured yields, but are expected to overestimate $E_{PdV,hs}$ since they cannot properly incorporate residual kinetic energy. This estimate is given in Table 4 as an upper bound.

We have thus develop four methodologies for estimating $E_{PdV,hs}$. In the main analysis we use a combination of the empirical piston

model estimate as the more pessimistic data-based inference, and use the 2-D simulated $E_{PdV,hs}$ as the most robust computational description of the experiments.

Modified Hurricane metric At peak burn, the time-rate of change of hot-spot volume, dV/dt, and therefore the heating-rate is nearly zero, so time integration is needed. Mathematically, a statement of a burning plasma appropriate for ICF is

$$\int_0^{t_{pf}} P_\alpha dt > -\int_0^{t_{minV}} \frac{P}{m} dV. \tag{13}$$

where t_{pf} is the time of peak fusion rate, and t_{minV} is the time of minimum hot-spot volume.

The integrals in Eq. 13 are easily approximated[2] without knowing the details of the actual implosion using the mathematical method of Steepest Descent; assuming that the thermodynamic quantities of interest, such as $T, P, \rho, \cdots$, are impulsive, being highly peaked around the time of stagnation. Ultimately, the solution to Eq. 13, in terms of only burn-average hot-spot areal density, ρR_{hs}, T_i, and v_{imp} is Eq. 1 after a correction to the original derivation.

A recent note from our colleagues at Los Alamos[47] discovered an arithmetic error in the derivation of the criteria as published in Ref. 3. The error is in going from Eq. 8 to Eq. 9 in Ref. 3 in which the conversion to peak temperature (T_0) to burn-averaged temperature (T_{hs}) should be, for $n \approx 4$,

$$\left.\frac{\langle\sigma v\rangle}{T_0}\right|_{T0} \approx \left(\frac{n+1}{n}\right)^{\frac{n-1}{2}} \left.\frac{\langle\sigma v\rangle}{T}\right|_{T_{hs}} \tag{14}$$

$$\approx 1.40 \left.\frac{\langle\sigma v\rangle}{T}\right|_{T_{hs}} \tag{15}$$

Additionally, we now believe that the inclusion of the alpha-stopping fraction f_α in Ref. 3 was inappropriate. When considering the temperature evolution of a defined mass (e.g. the self-heating criteria in Eq. 20) this is necessary because f_α is fundamentally the fraction of alpha energy deposited into that mass. On the other hand the burning plasma criteria is one on the energy of the hot spot,

$$E_{hs} = c_{DT} m_{hs} T_{hs} \tag{16}$$

and alphas which escape the hot spot still contribute to its energy via generation of additional hot-spot mass, as seen by examining the time derivative of the above:

$$\frac{dE_{hs}}{dt} = c_{DT}\left(m_{hs}\frac{dT_{hs}}{dt} + \frac{dm_{hs}}{dt}T_{hs}\right), \tag{17}$$

$$= m_{hs} f_\alpha Q_\alpha + m(1-f_\alpha)Q_\alpha, \tag{18}$$

$$= m_{hs} Q_\alpha. \tag{19}$$

Therefore the inclusion of f_α in a burning-plasma criteria is inappropriate. We note that not including a f_α factor is consistent with other criteria, e.g. Ref. 8. With these two modifications to the criteria published in Ref. 3 we use a new criteria (Eq. 1). This modified criteria is slightly more restrictive for the burning-plasma threshold in the regime relevant to these experiments.

Model uncertainties for Hurricane's metric The Hurricane metric[3] depends on more quantities than the Betti metric, although these quantities are more straightforward to infer than $E_{PdV,hs}$. The metric reduces to Eq. 1 where ρR_{hs} and v_{imp} are inferred as described previously, and T_i is measured. $\langle\sigma v\rangle$ contains some systematic uncertainty from the evaluation used. Data uncertainties are well-defined for T_i and in the inference of ρR_{hs} and v_{imp}, and are propagated as described in the next section; the inferred ρR_{hs} can also vary between models, which will be discussed.

Eq. 1 depends on the fusion reactivity; in this work we use the evaluation from Bosch and Hale [34]. Recent publications have presented alternative evaluations[48] which differ by $\sim 2\%$. We note that the inferred $\rho R \propto 1/\sqrt{\langle\sigma v\rangle}$ from Eq. 2, so the condition in Eq. 1 depends on the reactivity as $1/\sqrt{\langle\sigma v\rangle}$. f_α is also weakly increasing with ρR, leading to the condition being slightly less than square-root dependent on $\langle\sigma v\rangle$, so this criteria has $< 1\%$ uncertainty from the choice of $\langle\sigma v\rangle$ evaluation.

The Hurricane criteria is sensitive to the inferred hot-spot ρR, which can vary between models depending on the spatial dependence of ρ. As shown in Table 3, the 0-D and 1-D hot-spot models agree quite well. We also check these values using a 3-D reconstruction of the hot spot density and temperature profiles [a yet unpublished method of L. Divol, but briefly described in Ref. 37], for N201101 this gives a value of $\rho R_{hs} \sim 0.36 - 0.38$ g/cm^2 to the 1 keV contour for N201101 and $\rho R_{hs} \sim 0.35 - 0.36$ g/cm^2 for N201122. These values are consistent with the simple models described earlier.

Self-heating regime The hot-spot per unit mass power balance is:

$$c_{DT}\frac{dT}{dt} = f_\alpha P_\alpha - f_b P_b - P_e - \frac{P}{m}\frac{dV}{dt}, \tag{20}$$

which describes the temporal evolution of the temperature (T) in terms of the balance of self heating (P_α) vs bremsstrahlung (P_b) and electron conduction (P_e) losses plus PdV work. Here, electron conduction losses are calculated relative to a hot spot boundary that is defined relative to a fraction of the peak burn rate or a specified ion temperature. Thermal conduction cools the hot spot while increasing the mass of the hot spot. Since the fusion burn rate is more strongly dependent on the temperature of the spot than its mass in the temperature range achieved by compression alone, alpha heating must provide sufficient heating for the hot spot temperature to increase in the presence of this conduction into an increasing mass. Note that hot-spot volume change, dV/dt, is negative on implosion increasing T. During expansion the PdV term becomes an energy loss term. The bremsstrahlung loss can be enhanced beyond the emission of clean DT by the presence of high-Z contamination of the DT (i.e. mix), by a fraction f_b. In Eq. 20 f_α is the fraction of alpha particles stopped in the hot spot, evaluated using fits with modern stopping-power theory[49].

Uncertainty analysis We perform uncertainty analysis for all hot-spot quantities by propagating the normally-distributed uncertainties in measured quantities through the 0-D and 1-D models described earlier. The model input parameters are those that fully describe the system, and are constrained by the measured yield, ion temperature, burn widths (from both x rays and γ rays), and volume from the 17% contour of neutron emissivity. Distributions of model parameters are generated using Markov Chain Monte Carlo (MCMC), calculated with the `tensorflow`[50] probability package. The log-likelihood function for MCMC is defined by the measurements and calculated with the log-likelihood function

$$-\frac{1}{2}\sum_i \left(\frac{m_i - y_i}{\delta y_i}\right)^2, \tag{21}$$

which is summed over all observables (i) where m_i is the model value, y_i is the measured value, and δy_i is the uncertainty in the measurement. This methodology produces full distributions of the model parameters including any correlations, from the model parameter distributions we generate full distributions of all hot-spot parameters, some of which exhibit correlation, such as in the temperature and areal density required to evaluate the Hurricane metric, which are partially anti-correlated (evident in Fig. 3a). Other inferences, such as the implosion velocity or kinetic energy, are treated with normally-distributed uncertainties that are uncorrelated with the hot-spot inferences.

Power balance relations In evaluating the power-balance relations relevant to Eq. 20 we use the following expressions for the individual terms:

$$P_\alpha = 8.2 \times 10^{24} \rho \langle \sigma v \rangle, \quad (22)$$

$$P_b = 3.1 \times 10^{7} \rho \sqrt{T}, \quad (23)$$

$$P_e = 5.9 \times 10^{3} \frac{T^{3.5}}{\rho R^2}. \quad (24)$$

In these expressions the specific powers are given in units of GJ/(g·s) and thus are multiplied by the inferred hot-spot mass to obtain power. ρ is the hot-spot mass in g/cm^3, $\langle \sigma v \rangle$ is the fusion reactivity evaluated as a function of temperature in cm^3/s, T is the temperature in keV, and ρR is the hot-spot areal density in g/cm^2. The self-heating power P_α is multiplied by the fraction of alpha-particle energy deposited in the hot spot (f_α) using the evaluation published in Ref. 49; for all four experiments $f_\alpha \sim 0.77 - 0.80$.

Data availability Raw data were generated at the National Ignition Facility. Derived data supporting the findings of this study are available from the corresponding authors upon request.